

Vortex states and spin textures of rotating spin-orbit-coupled Bose-Einstein condensates in a toroidal trap

Huan Wang,¹ Linghua Wen,^{1,*} Hui Yang,¹ Chunxiao Shi,¹ and Jinghong Li²

¹*College of Science, Yanshan University, Qinhuangdao 066004, China*

²*College of Environment and Chemical Engineering,
Yanshan University, Qinhuangdao 066004, China*

(Dated: August 30, 2018)

We consider the ground-state properties of Rashba spin-orbit-coupled pseudo-spin-1/2 Bose-Einstein condensates (BECs) in a rotating two-dimensional (2D) toroidal trap. In the absence of spin-orbit coupling (SOC), the increasing rotation frequency enhances the creation of giant vortices for the initially miscible BECs, while it can lead to the formation of semiring density patterns with irregular hidden vortex structures for the initially immiscible BECs. Without rotation, strong 2D isotropic SOC yields a heliciform-stripe phase for the initially immiscible BECs. Combined effects of rotation, SOC, and interatomic interactions on the vortex structures and typical spin textures of the ground state of the system are discussed systematically. In particular, for fixed rotation frequency above the critical value, the increasing isotropic SOC favors a visible vortex ring in each component which is accompanied by a hidden giant vortex plus a (several) hidden vortex ring(s) in the central region. In the case of 1D anisotropic SOC, large SOC strength results in the generation of hidden linear vortex string and the transition from initial phase separation (phase mixing) to phase mixing (phase separation). Furthermore, the peculiar spin textures including skyrmion lattice, skyrmion pair and skyrmion string are revealed in this system.

PACS numbers: 67.85.-d, 03.75.Kk, 03.75.Lm, 03.75.Mn

I. INTRODUCTION

Spin-orbit coupling (SOC) of a quantum particle plays a key role in many physical phenomena, including fine structures of atomic spectra, spin Hall effect [1], topological insulators [2] and topological superconductors [3]. In general, the SOC strengths in solid materials are fixed, and the observation of SOC effects is hindered by unavoidable impurities and disorder. In contrast, the spin-orbit coupled ultracold atomic gases demonstrated by the milestone experiments [4–7] offer an extremely clean platform with full controllability to explore novel macroscopic quantum phenomena and quantum topological states [8, 9], especially for bosons [10–17]. Recently, the two-dimensional (2D) SOC for boson gases and for fermion gases have been realized, respectively [18, 19], which is crucial in studying the exotic properties of high-dimensional topological matter. Of particular interest are the topological excitations in rotating Bose-Einstein condensates (BECs) with SOC. Relevant studies show that the spin-1/2 BECs with SOC in a rotating harmonic trap support the formation of half-quantum vortex, giant vortex, skyrmion, and multidomain pattern [20–27].

However, there are few studies so far on the ground-state properties of rotating spin-orbit-coupled BECs in a toroidal trap. In fact, various trapping potentials may significantly affect the ground states and dynamic properties of the BECs [28–32], which leads to a rich physics. In this work, we investigate the vortex states and spin textures of rotating BECs with Rashba SOC in a toroidal trap. As a non-trivial geometry, toroidal trap can be easily created in current experiments [33–37], and it provides us a unique platform to investigate the exotic properties of quantum superfluids. Therefore our work is experimentally feasible and allows to be tested in future experiments. We show that increasing 2D isotropic SOC can enhance the formation of visible vortex ring, hidden giant vortex (or hidden singly quantized vortices), and spin domain walls for large rotation frequency above the critical value. In the nonrotating limit, strong 2D isotropic SOC generates a heliciform-stripe phase for the initially separated condensates in a toroidal trap. In addition, large strength of the 1D SOC leads to the creation of hidden linear vortex string and the transition from initial phase separation (or phase mixing) to phase mixing (or phase separation). Moreover, the combined effects of the rotation, SOC, and interparticle interactions on the ground-state properties of the system are discussed.

The paper is organized as follows. In section 2, the model Hamiltonian is introduced and the coupled dynamic equations are given. The topological structures and typical spin textures of the ground state of the system are

*Electronic address: linghuawen@ysu.edu.cn

described and analyzed in section 3. Conclusions are outlined in section 4.

II. THEORETICAL MODEL

We consider a quasi-two-dimensional (x, y) rotating spin-orbit-coupled BEC in a toroidal trap. The model Hamiltonian for the interacting pseudo-spin-1/2 BEC is given by

$$\hat{H} = \int dx dy \hat{\psi}^\dagger \left[-\frac{\hbar^2 \nabla^2}{2m} + V(r) + g_1 \hat{n}_1^2 + g_2 \hat{n}_2^2 + 2g_{12} \hat{n}_1 \hat{n}_2 - \Omega \hat{L}_z + v_{SO} \right] \hat{\psi}, \quad (1)$$

where $\hat{\psi} = [\hat{\psi}_1(r), \hat{\psi}_2(r)]^T$ denotes collectively the spinor Bose field operators with 1 and 2 corresponding to spin-up and spin-down, respectively. $\hat{n}_1 = \hat{\psi}_1^\dagger \hat{\psi}_1$ and $\hat{n}_2 = \hat{\psi}_2^\dagger \hat{\psi}_2$ are the density operators of the particle numbers for spin-up and spin-down atoms, respectively. $g_j = 4\pi a_j \hbar^2/m$ ($j = 1, 2$) and $g_{12} = 2\pi a_{12} \hbar^2/m$ represent the intra- and intercomponent coupling strengths, where m is the atomic mass, a_j ($j = 1, 2$) and a_{12} are the s -wave scattering lengths between intra- and intercomponent atoms. Ω is the rotation angular velocity along the z direction, and $\hat{L}_z = -i\hbar(x\partial_y - y\partial_x)$ is the z component of the angular-momentum operator. The Rashba SOC term is given by $v_{SO} = -i\hbar(\lambda_y \hat{\sigma}_x \partial_y - \lambda_x \hat{\sigma}_y \partial_x)$ with $\hat{\sigma}_{x,y}$ being Pauli matrices and λ_x and λ_y being the SOC strengths in the x and y directions. The external toroidal potential is expressed as [38]

$$V(r) = \frac{1}{2} m \omega_\perp^2 \left[V_0 \left(\frac{r^2}{a_0^2} - a_0 r_0 \right)^2 \right] = \frac{1}{2} \hbar \omega_\perp \left[V_0 \left(\frac{r^2}{a_0^2} - r_0 \right)^2 \right], \quad (2)$$

where ω_\perp is the radial oscillation frequency, $a_0 = \sqrt{\hbar/m\omega_\perp}$, $r = \sqrt{x^2 + y^2}$. V_0 and r_0 are dimensionless constants which characterize the width and the central height of the toroidal potential. $(\pm a_0 \sqrt{r_0}, 0)$ and $(0, \hbar \omega_\perp V_0 r_0^2/2)$ represent the lowest point and the highest one of the potential well, respectively. The normalization condition of the system reads

$$\int [|\psi_1|^2 + |\psi_2|^2] dx dy = N, \quad (3)$$

where ψ_j ($j = 1, 2$) is the wave function of component j , and N is the number of atoms. By introducing the notations $\tilde{t} = \omega_\perp t$, $\tilde{r} = r/a_0$, $\tilde{V} = V/\hbar \omega_\perp$, $\tilde{\Omega} = \Omega/\omega_\perp$, $\tilde{L}_z = L_z/\hbar$, and $\tilde{\psi}_j = \psi_j a_0/\sqrt{N}$ ($j = 1, 2$), we obtain the dimensionless coupled Gross-Pitaevskii (GP) equations for the dynamics of the system in terms of the variational principle,

$$i\partial_t \psi_1 = \left(-\frac{1}{2} \nabla^2 + V + \beta_{11} |\psi_1|^2 + \beta_{12} |\psi_2|^2\right) \psi_1 - \Omega L_z \psi_1 + (\lambda_x \partial_x - i\lambda_y \partial_y) \psi_2, \quad (4)$$

$$i\partial_t \psi_2 = \left(-\frac{1}{2} \nabla^2 + V + \beta_{12} |\psi_1|^2 + \beta_{22} |\psi_2|^2\right) \psi_2 - \Omega L_z \psi_2 - (\lambda_x \partial_x + i\lambda_y \partial_y) \psi_1, \quad (5)$$

where the tilde is omitted for simplicity. β_{jj} ($j = 1, 2$) and $\beta_{12} = \beta_{21}$ are the dimensionless intra- and intercomponent interaction strengths.

In the frame of nonlinear Sigma model [25, 39, 40], we can introduce a normalized complex-valued spinor $\chi = [\chi_1, \chi_2]^T$ with $|\chi_1|^2 + |\chi_2|^2 = 1$. The total density of the system is given by $\rho = |\psi_1|^2 + |\psi_2|^2$, and the corresponding two-component wave functions are $\psi_1 = \sqrt{\rho} \chi_1$ and $\psi_2 = \sqrt{\rho} \chi_2$, respectively. The spin density is defined as $\mathbf{S} = \bar{\chi} \boldsymbol{\sigma} \chi$, where $\boldsymbol{\sigma} = (\sigma_x, \sigma_y, \sigma_z)$ are the Pauli matrices, and the components of \mathbf{S} are expressed as

$$S_x = \chi_1^* \chi_2 + \chi_2^* \chi_1, \quad (6)$$

$$S_y = i(\chi_2^* \chi_1 - \chi_1^* \chi_2), \quad (7)$$

$$S_z = |\chi_1|^2 - |\chi_2|^2, \quad (8)$$

with $|\mathbf{S}|^2 = S_x^2 + S_y^2 + S_z^2 = 1$. In order to describe the spacial distribution of the topological structure, we introduce a topological charge density

$$q(r) = \frac{1}{4\pi} \mathbf{S} \cdot \left(\frac{\partial \mathbf{S}}{\partial x} \times \frac{\partial \mathbf{S}}{\partial y} \right), \quad (9)$$

then we can obtain the topological charge Q by calculating the whole space integral of $q(r)$,

$$Q = \int q(r) dx dy. \quad (10)$$

III. RESULTS AND DISCUSSION

In what follows, we numerically solve the 2D coupled GP equations (4) and (5). We obtain the minimizing energy state (i.e., the ground state) of the system by using the imaginary-time propagation method [15] based on the Peaceman-Rachford method [41, 42]. Recently, a phase diagram for a nonrotating spin-orbit-coupled BEC in a harmonic trap has been discussed in the literature [25]. In the present work, we investigate systematically the combined effects of rotation, SOC and interatomic interactions on the ground state of the BECs in a toroidal trap. In our simulation, the typical parameters of the toroidal potential are chosen as $V_0 = 0.5$ and $r_0 = 3$, the intraspecies interactions are fixed as $\beta_{11} = \beta_{22} = 100$. It is shown that system can exhibit rich and exotic topological structures and spin textures due to the topology difference between the toroidal and the harmonic traps.

A. Rotation effect

Firstly, we consider the effect of rotation on the ground state of a toroidal interacting spin-1/2 BEC in the absence of SOC. Figure 1 shows the density distributions [(a), (b) and (d)] and phase distributions [(c) and (e)] of the ground states of the system, where $\beta_{11} = \beta_{22} = 100$, $\beta_{12} = 50$ (the top two rows), and $\beta_{12} = 150$ (the bottom two rows). The rotation frequencies are $\Omega = 0$ [column (a)], $\Omega = 0.8$ [the top two rows of (b)-(c)], $\Omega = 1.2$ [the bottom two rows of (b)-(c)], and $\Omega = 2$ [(d)-(e)], respectively. Here the odd and even rows denote component 1 and component 2, respectively.

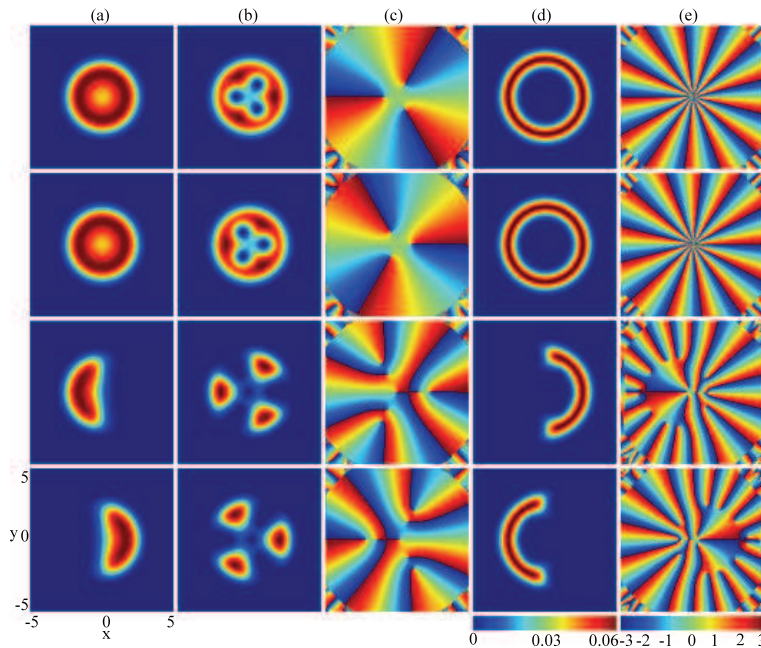


FIG. 1: (Color online) Density distributions [(a), (b), and (d)] and phase distributions [(c) and (e)] for the ground states of rotating toroidal spin-1/2 BECs in the absence of SOC. Here the odd rows correspond to component 1, while the even ones correspond to component 2. The interaction parameters are $\beta_{11} = \beta_{22} = 100$, $\beta_{12} = \beta_{21} = 50$ (the top two rows) and $\beta_{12} = \beta_{21} = 150$ (the bottom two rows), which correspond to phase mixing and phase separation of a nonrotating system, respectively. The rotation frequency are $\Omega = 0$ [column (a)], $\Omega = 0.8$ [the top two rows of (b)-(c)], $\Omega = 1.2$ [the bottom two rows of (b)-(c)], and $\Omega = 2$ [(d)-(e)]. The horizontal and vertical coordinates x and y are in units of a_0 .

As shown in figure 1(a), the two components of the nonrotating BEC display typical phase mixing (top two rows) and phase separation (bottom two rows), due to the interatomic interactions satisfying $\beta_{11}\beta_{22} > \beta_{12}^2$ and $\beta_{11}\beta_{22} < \beta_{12}^2$, respectively. For the convenience of discussion, in the following texts we call the two phases briefly initial phase mixing and initial phase separation, respectively. In the case of initial phase mixing, when $\Omega = 0.8$ the rotation driving inputs sufficient angular momentum such that three visible vortices [30, 42] occur in each component and constitute a triangular vortex lattice (Abrikosov lattice), where the two visible vortex lattices are staggered each other [see the top two rows in (b)-(c)]. When $\Omega = 2$ a giant vortex (a multiply-quantized vortex) is generated in each component [see the top two rows of (d)-(e)], which is inaccessible in a harmonically trapped BEC because for

$\Omega \rightarrow 1$ the resulting centrifugal effect would cancel the radial confinement and the Thomas-Fermi (TF) radius of the BEC would diverge. In the case of initial phase separation, when $\Omega = 1.2$ the component densities become separated petals, where the hidden vortices [30, 42–44] form a regular vortex cluster. With the further increase of rotation frequency, e.g., $\Omega = 2$, the component densities form two butt-joint semi-rings and the hidden vortices display complex topological structures, which can be seen in the bottom two rows of (d)-(e).

B. The effect of SOC

Secondly, we consider the effect of SOC on the ground state of the nonrotating spin-1/2 BEC in a toroidal potential. The main results are illustrated in figure 2. For 2D weak SOC, e.g., $\lambda_x = \lambda_y = 1$, the ground-state structure of the system with an initial phase mixing is similar to that with an initial phase separation except for the difference between the density mixing and the density separation, where few ghost vortices are generated in each component [see the left four columns in (a)-(b)]. However, for 2D strong SOC, e.g., $\lambda_x = \lambda_y = 10$, there exists a remarkable difference between the ground-state structure in the case of initial phase mixing and that in the case of initial phase separation [see the left four columns in (c)-(d)]. For the former case, a visible vortex string is formed along the $y = 0$ axis in each component, and the two vortex strings are separated spatially due to the strong SOC. In contrast, for the latter case, the two components display spatially separated and heliciform stripe structures. When there is only 1D SOC in the BEC, e.g., $\lambda_x = 10$ and $\lambda_y = 0$, the system exhibits either a fully mixed phase with a fringe-shape phase distribution for weak interspecies repulsion or a separated stripe phase along the x direction for strong interspecies repulsion, which are referred as Thomas-Fermi (TF) phase (plane wave phase) and stripe phase [15], respectively. As for the other values of λ_x and $\lambda_y = 0$, our simulation shows that the density and phase patterns are similar to those in the right two columns of figure 2. If the 1D SOC is along the y direction, e.g., $\lambda_x = 0$ and $\lambda_y = 10$, the density and phase distributions will correspondingly rotate 90 degrees due to the rotation of the SOC.

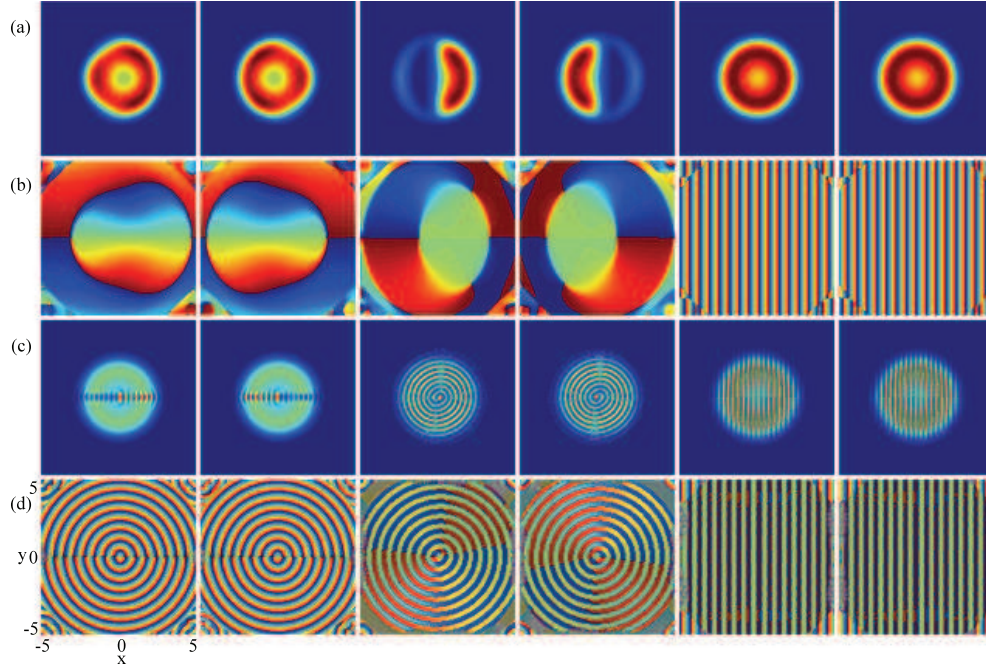


FIG. 2: (Color online) Density distributions [(a) and (c)] and phase distributions [(b) and (d)] for the ground states of nonrotating SOC spin-1/2 BECs in a toroidal trap. The odd and even columns correspond to component 1 and component 2, respectively. The left two columns: $\beta_{12} = 50$, (a)-(b) $\lambda_x = \lambda_y = 1$, and (c)-(d) $\lambda_x = \lambda_y = 10$. The middle two columns: $\beta_{12} = 150$, (a)-(b) $\lambda_x = \lambda_y = 1$, and (c)-(d) $\lambda_x = \lambda_y = 10$. The right two columns: $\lambda_x = 10$, $\lambda_y = 0$, (a)-(b) $\beta_{12} = 50$, and (c)-(d) $\beta_{12} = 150$. The horizontal and vertical coordinates x and y are in units of a_0 .

C. The combined effects of rotation, SOC and interatomic interactions

1. Fixed rotation frequency

Next, we investigate the combined effects of SOC, rotation and interatomic interactions on the ground state of the system. Figure 3 shows the density distributions and phase distributions for the ground states of rotating toroidal spin-1/2 BECs, where $\Omega = 0.9$. The strengths of the 2D SOC for the initial phase mixing with $\beta_{12} = 50$ in rows (a)-(b) are $\lambda_x = \lambda_y = 1$ and $\lambda_x = \lambda_y = 10$, and those for the initial phase separation with $\beta_{12} = 150$ in rows (c)-(e) are $\lambda_x = \lambda_y = 0.2$, $\lambda_x = \lambda_y = 1$ and $\lambda_x = \lambda_y = 8$, respectively. The columns (from left to right) represent $|\psi_1|^2$, $|\psi_2|^2$, $\arg\psi_1$, $\arg\psi_2$, $|\psi_1|^2 + |\psi_2|^2$, and $|\psi_1|^2 - |\psi_2|^2$, respectively.

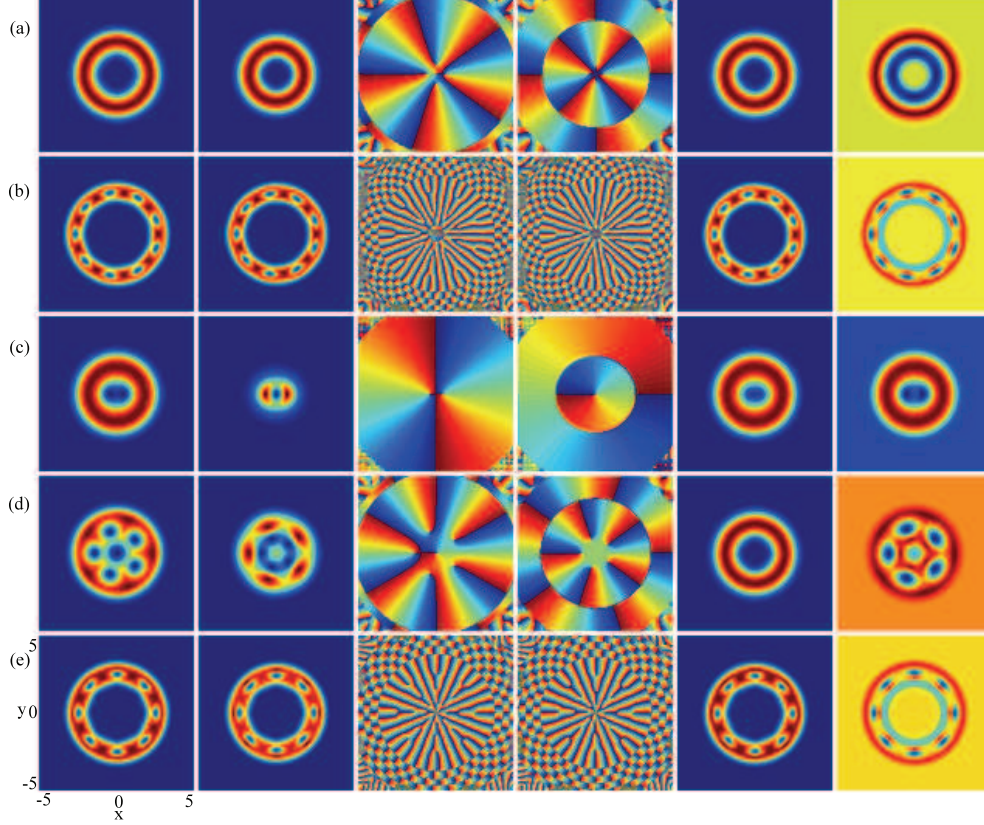


FIG. 3: (Color online) Ground states of rotating interacting spin-1/2 BECs with SOC in a toroidal trap, where $\Omega = 0.9$. (a) $\beta_{12} = 50$, $\lambda_x = \lambda_y = 1$, (b) $\beta_{12} = 50$, $\lambda_x = \lambda_y = 10$, (c) $\beta_{12} = 150$, $\lambda_x = \lambda_y = 0.2$, (d) $\beta_{12} = 150$, $\lambda_x = \lambda_y = 1$, and (e) $\beta_{12} = 150$, $\lambda_x = \lambda_y = 8$. The columns (from left to right) represent $|\psi_1|^2$, $|\psi_2|^2$, $\arg\psi_1$, $\arg\psi_2$, $|\psi_1|^2 + |\psi_2|^2$, and $|\psi_1|^2 - |\psi_2|^2$, respectively. The horizontal and vertical coordinates x and y are in units of a_0 .

As shown in figures 3(a) and 3(c), the density distributions and phase distributions for relatively weak SOC and large rotation frequency display remarkable difference between the case of initial phase mixing and that of initial phase separation. In figure 3(a), the two large density holes in the two components are not the normal giant vortices observed in rotating harmonically trapped BECs with SOC [20, 22] but a hidden triangular vortex lattice and a vortex ring, respectively. While in figure 3(c) the two component densities exhibit obvious phase separation, where the vortices in the two components develop into an interlaced vortex array. For large SOC, we observed that there was an enhanced overlap of the density distributions and the phase distributions between the two components. This feature exists not only for the case of $\beta_{12} < \beta_{11}$ but also for the case of $\beta_{12} > \beta_{11}$ [see figures 3(b), 3(d) and 3(e)]. Here the visible vortices form ringlike structures. The region of the large density hole is occupied by a central hidden giant vortex and a (several) hidden vortex ring(s) [see figures 3(b) and 3(e)]. The ringlike visible vortex configuration has also been found in a two-component spin-orbit coupled BEC subject to an in-plane gradient magnetic field [45]. However, the present toroidal system can exhibit more rich and complex topological structures due to the interplay among rotation, interatomic interactions, SOC, and toroidal confinement.

In addition, a topology transition is indicated in the system. We take the case of $\beta_{12} > \beta_{11}$ as an example. In figure

3(c), there exist two vortices around the center of component 1. For comparison, there are five visible vortices around the center visible vortex of component 1 in figure 3(d) and eight nearest hidden vortices around the center giant vortex of component 1 in figure 3(e), respectively. Therefore these patterns display the transition of the topological structure as the strength of SOC increases, which indicates that SOC can be used to control the topological structure of the rotating toroidal BEC. Note that there are obvious singular points in the total density $|\psi_1|^2 + |\psi_2|^2$ of the system (see the fifth column). Thus the topological defects in the present system are different from the common coreless vortices [46] or the so-called Anderson-Toulouse vortices [47].

The corresponding spin-density distributions are shown in figure 4. In the pseudo-spin representation, the blue region denotes spin-down and the red region denotes spin-up. To understand the interesting spin structures, we take the case of $\Omega = 0.9$, $\beta_{12} = 50$, and $\lambda_x = \lambda_y = 1$ as a typical example. From S_z in figure 4(a), the spin continuously turn from down to up along the radial direction and then gradually turn back to down. At the same time, S_x obeys an odd parity distribution along the x direction and an even parity distribution along the y direction, but the situation is the reverse for S_y .

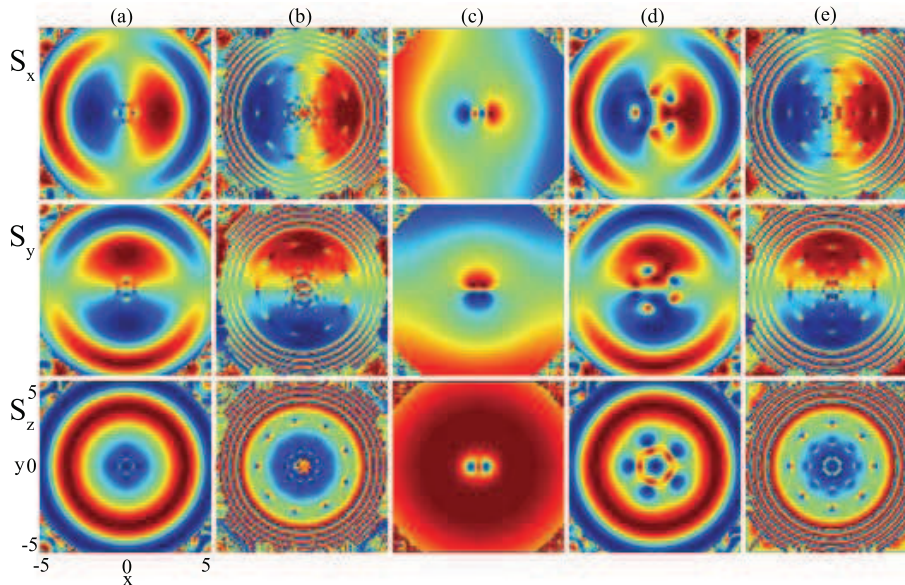


FIG. 4: (Color online) Spin densities of the rotating interacting spin-1/2 BECs with SOC in a toroidal trap, where $\Omega = 0.9$, and columns (a)-(e) correspond to rows (a)-(e) in figure 3, respectively. The rows (from top to bottom) denote S_x , S_y and S_z components of the spin density vector, respectively. The horizontal and vertical coordinates x and y are in units of a_0 .

Displayed in figure 5(a) and figures 5(b)-5(c) are the topological charge density and the spin texture for the parameters in figure 4(a), respectively. Obviously, there are five radial-out skyrmions [24, 48–50] in figure 5(b) which constitute a skyrmion lattice in spin representation. The larger SOC leads to the generation of a more complex skyrmion lattice (including more skyrmions even giant skyrmion [51]) through the strong interaction between the ‘spin’ angular momentum and orbit angular momentum of the atoms, where the necklace-like distribution in the spin density becomes more distinct. This characteristic is present evidently for both the cases of $\beta_{12} < \beta_{11}$ and $\beta_{12} > \beta_{11}$ [see figures 4(b), 4(d) and 4(e)]. In particular, we find that at certain parameters the rotating toroidal system with SOC supports a skyrmion pair. Figures 5(e)-5(f) show the spin texture and its local amplification at $\Omega = 0.9$, $\beta_{12} = 150$, and $\lambda_x = \lambda_y = 0.2$, and figure 5(d) gives the corresponding topological charge density. We see that the spin texture exhibits a radial(out)-radial(out) skyrmion configuration, which is quite different from the normal seven basic skyrmion configurations [24] of rotating spin-orbit-coupled BECs in a harmonic trap. Our numerical calculation shows that the topological charge approaches $|Q| = 2$, and thus we may call it skyrmion pair.

2. Fixed intercomponent interaction

Now we discuss the ground state of the system at fixed intercomponent interaction. Figure 6 and figure 7 depict the density distributions and phase distributions obtained under various strengths of SOC and rotation frequencies for the initially miscible BECs ($\beta_{12} = 50$) and the initially immiscible BECs ($\beta_{12} = 150$), respectively. In the initially miscible case of $\beta_{12} = 50$, when the SOC strength is relatively weak and the rotation frequency is small, there is a

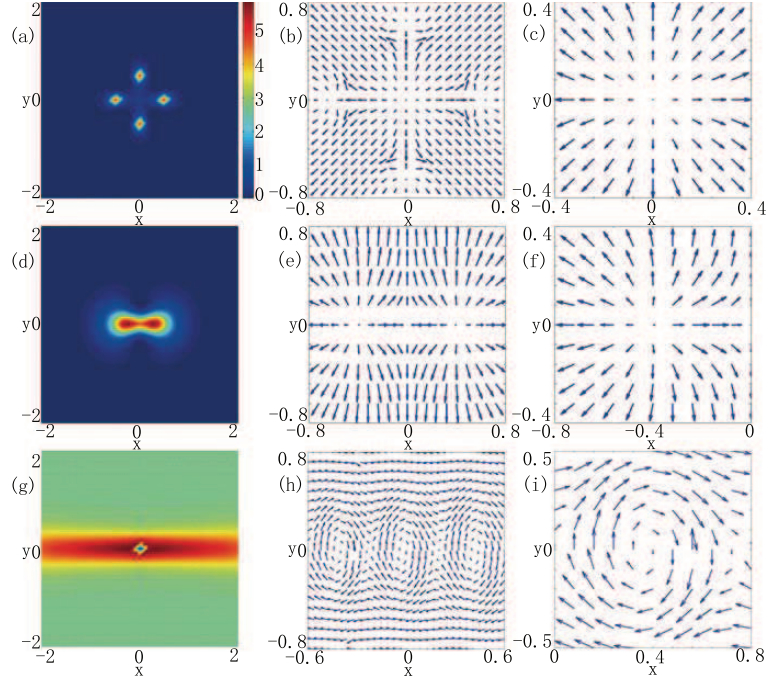


FIG. 5: (Color online) Topological charge densities and spin textures of rotating spin-1/2 BEC with SOC in a toroidal trap. The left column denotes topological charge density, the middle column is the corresponding spin texture, and the right column is the local amplification of the spin texture. (a)-(c) $\Omega = 0.9$, $\beta_{12} = 50$, $\lambda_x = \lambda_y = 1$, (d)-(f) $\Omega = 0.9$, $\beta_{12} = 150$, $\lambda_x = \lambda_y = 0.2$, and (g)-(i) $\Omega = 1.2$, $\beta_{12} = 150$, $\lambda_x = 2$, $\lambda_y = 0$. The horizontal and vertical coordinates x and y are in units of a_0 .

typical triangular vortex lattice in component 1 and a doubly quantized vortex in component 2. With the increase of rotation frequency, the trap center region is pinned by a triply quantized vortex for component 1 and a doubly quantized vortex for component 2. At the same time, a vortex ring is formed on the periphery of the giant vortex in each component. For large SOC strength, each component forms a complex topological structure composed of laminar visible vortex ring(s) and a large density hole. Note that the large density hole represents a giant vortex plus hidden vortex ring(s) rather than a pure giant vortex which is observed in conventional rotating BECs [52]. In addition, the density distributions and phase distributions for the two components become similar. Therefore the topological structure of the system is strongly influenced by the interplay among the SOC, rotation frequency, the interparticle interactions, and the toroidal confinement.

In the initially immiscible case of $\beta_{12} = 150$, when the SOC is relatively weak and the rotation frequency is small, the two components exhibit remarkable phase separation as shown in figure 7(a). The topological structure of the system in figure 7(a) is a typical Anderson-Toulouse coreless vortex [47], where the core of the circulating external component is filled with the other nonrotating component. With the further increase of rotation frequency, each component of the system evolves from a standard triangular vortex lattice into a special topological configuration which is comprised of an exterior vortex ring and a central vortex (or giant vortex) due to the presence of central barrier [see figures 7(b) and 7(c)]. For large SOC strength and small rotation frequency, the visible vortices tend to be elongated along the radius and linked one after another [figure 7(d)]. When the rotation frequency increases, the elongated effect of the visible vortices becomes deformed and eventually disappears, and the final topological structure of the system is similar to that in the initially miscible case. From figure 2 to figure 7, we show that the rich topological structures of the rotating toroidal BECs with SOC are determined by the interplay among the SOC, the rotation frequency, and the interatomic interactions, especially for the SOC strength.

3. One-dimensional SOC

Finally, we study the ground-state structures of rotating toroidal BECs in the presence of 1D SOC, where the relevant parameters are $\beta_{12} = 150$, $\lambda_x = 2$, $\lambda_y = 0$, $\Omega = 0.5$ [figure 8(a)] and $\Omega = 1.2$ [figure 8(b)]. The columns (from left to right) in figures 8(a)-8(b) represent $|\psi_1|^2$, $|\psi_2|^2$, $\arg\psi_1$, $\arg\psi_2$, $|\psi_1|^2 + |\psi_2|^2$, and $|\psi_1|^2 - |\psi_2|^2$, respectively. The corresponding spin density components S_x , S_y and S_z are shown in the left three columns and the right three

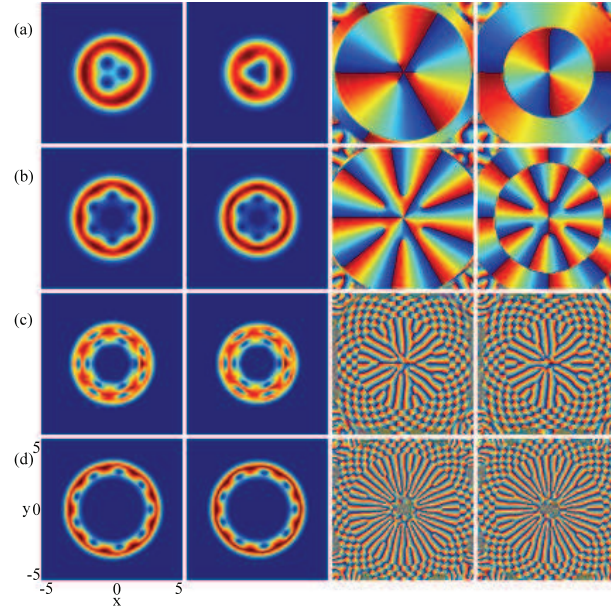


FIG. 6: (Color online) Ground states of rotating interacting spin-1/2 BECs with SOC in a toroidal trap, where $\beta_{12} = 50$. (a) $\lambda_x = \lambda_y = 1$, $\Omega = 0.4$, (b) $\lambda_x = \lambda_y = 1$, $\Omega = 1.2$, (c) $\lambda_x = \lambda_y = 10$, $\Omega = 0.4$, and (d) $\lambda_x = \lambda_y = 10$, $\Omega = 1.2$. The columns (from left to right) represent $|\psi_1|^2$, $|\psi_2|^2$, $\arg\psi_1$, and $\arg\psi_2$, respectively. The horizontal and vertical coordinates x and y are in units of a_0 .

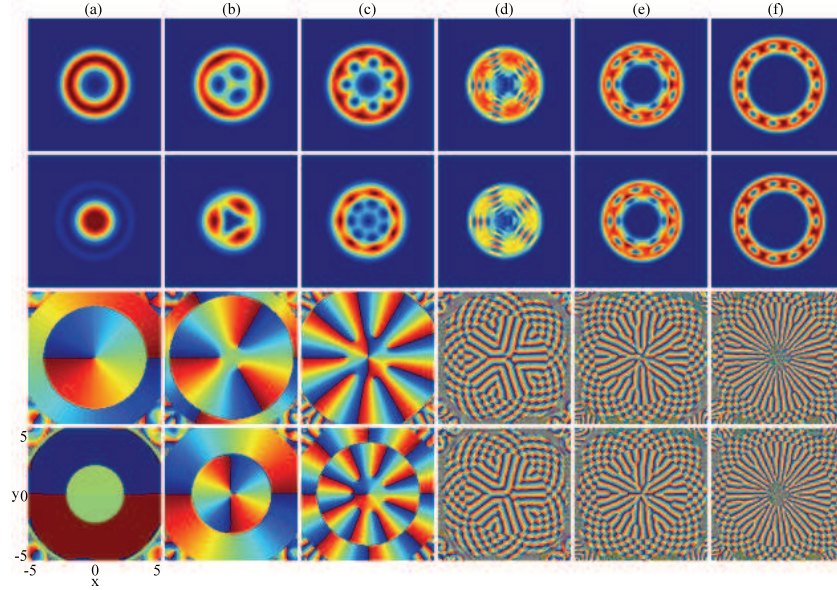


FIG. 7: (Color online) Ground states of rotating interacting spin-1/2 BECs with SOC in a toroidal trap, where $\beta_{12} = 150$. (a) $\lambda_x = \lambda_y = 1$, $\Omega = 0.2$, (b) $\lambda_x = \lambda_y = 1$, $\Omega = 0.6$, (c) $\lambda_x = \lambda_y = 1$, $\Omega = 1.2$, (d) $\lambda_x = \lambda_y = 10$, $\Omega = 0.2$, (e) $\lambda_x = \lambda_y = 10$, $\Omega = 0.6$, and (f) $\lambda_x = \lambda_y = 10$, $\Omega = 1.2$. The rows (from top to bottom) represent $|\psi_1|^2$, $|\psi_2|^2$, $\arg\psi_1$, and $\arg\psi_2$, respectively. The horizontal and vertical coordinates x and y are in units of a_0 .

columns in figure 8(c), respectively. When $\Omega = 0.5$, there is an obvious visible vortex string along the $y = 0$ axis in each component due to the 1D SOC along the x direction, and the system displays an evident phase separation [see figure 8(a)]. As shown in figure 8(b), besides the vortex string along the $y = 0$ axis, there exists a doubly-quantized vortex in the trap center and a vortex distribution along the $x = 0$ axis in individual components. The main reason is that for large rotation frequency $\Omega = 1.2$ the x -direction vortex string resulted from the combined effect of 1D SOC and rotation can only carry partial angular momentum and the remain angular momentum is inevitably carried by the central giant vortex and the transverse vortices beside the $y = 0$ axis.

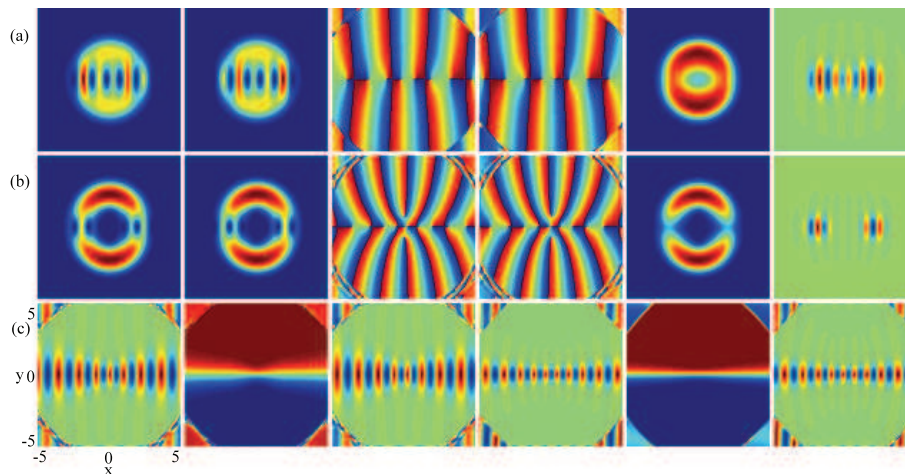


FIG. 8: (Color online) Ground states and spin densities of rotating interacting BECs with 1D SOC. The six columns (from left to right) in rows (a)-(b) represent $|\psi_1|^2$, $|\psi_2|^2$, $\arg\psi_1$, $\arg\psi_2$, $|\psi_1|^2 + |\psi_2|^2$, and $|\psi_1|^2 - |\psi_2|^2$, respectively. The left three and right three columns in (c) denote S_x , S_y and S_z components of spin density vectors corresponding to the first and the second rows, respectively. Here the parameters are $\beta_{12} = 150$, $\lambda_x = 2$, and $\lambda_y = 0$. The rotation frequencies in (a) and (b) are $\Omega = 0.5$ and $\Omega = 1.2$, respectively. The horizontal and vertical coordinates x and y are in units of a_0 .

In the spin representation, the spin component S_y develops into two remarkable spin domains due to the phase separation of the two component densities, and the boundary between the two spin domains forms a spin domain wall with $|S_y| \neq 1$, which can be seen clearly in figure 8(c). It is well known that the spin domain wall for a nonrotating two-component condensate system is a typically classical Neel wall, where the spin flips only along the vertical direction of the wall. However, our numerical simulation of the spin texture shows that in the region of spin domain wall the spin flips not only along the y direction (the vertical direction of domain wall) but also along the x direction (the domain-wall direction), which implies that the observed spin domain wall is a new type of domain wall. The topological charge density and the spin texture for the case of $\beta_{12} = 150$, $\lambda_x = 2$, $\lambda_y = 0$ and $\Omega = 1.2$ are shown in figures 5(g)-5(i), where a special topological structure of skyrmion string is formed in the spin representation. In addition, the S_x and S_z components of the spin density display a chain structure, where S_x satisfies the even-parity distribution while S_z obeys the odd-parity distribution.

IV. CONCLUSION

In summary, we investigate systematically the ground state of rotating two-component BECs with Rashba spin-orbit coupling in a toroidal trap. The influence of rotation, SOC, and interatomic interactions on the ground state of the system is analyzed in detail. In the absence of SOC, large rotation velocity yields the formation of giant vortices for initially miscible two-component BECs. However, for initially immiscible two-component BECs rapid rotation can generate semiring density structures with irregular hidden vortices. In the absence of rotation, large strength of 2D isotropic SOC may result in a heliciform-stripe phase for initially separated two-component BECs. The combined effects of SOC, rotation, and interparticle interactions are discussed. For large rotation frequency, strong 2D SOC favors a ringlike visible vortex configuration, where the region of large density hole is occupied by a hidden giant vortex and a (several) hidden vortex ring(s). In particular, strong 1D anisotropic SOC leads to the generation of hidden linear vortex string and the transition between phase separation (phase mixing) and phase mixing (phase separation). In addition, complex spin topological structures, such as skyrmion pair, skyrmion string, and skyrmion lattice are found in the present system. This work provides exciting perspectives for topological excitations in quantum gases and condensed matter physics.

Note added: Recently, we became aware of two preprints by Zhang *et al.* [53] and White *et al.* [54], which have also studied some relevant properties of spin-orbit coupled BECs in a toroidal trap.

Acknowledgments

L.W. thanks Chuanwei Zhang, Hui Zhai, Yongping Zhang, Zhi-Fang Xu, and Xiang-Fa Zhou for helpful discussions. This work is supported by the National Natural Science Foundation of China (Grant No. 11475144), the Natural Science Foundation of Hebei Province of China (Grant No. A2015203037), and Ph.D. foundation of Yanshan University (Grant No. B846).

-
- [1] Xiao D, Chang M-C and Niu Q 2010 *Rev. Mod. Phys.* **82** 1959
 - [2] Qi X-L and Zhang S-C 2011 *Rev. Mod. Phys.* **83** 1057
 - [3] Read N and Green D 2000 *Phys. Rev. B* **61** 10267
 - [4] Lin Y-J, Jiménez-García K and Spielman I B 2011 *Nature (London)* **471** 83
 - [5] Wang P, Yu Z-Q, Fu Z, Miao J, Huang L, Chai S, Zhai H and J Zhang 2012 *Phys. Rev. Lett.* **109** 095301
 - [6] Cheuk L W, Sommer A T, Hadzibabic Z, Yefsah T, Bakr W S and Zwierlein M W 2012 *Phys. Rev. Lett.* **109** 095302
 - [7] Zhang J-Y, Ji S-C, Chen Z, Zhang L, Du Z-D, Yan B, Pan G-S, Zhao B, Deng Y-J, Zhai H, Chen S and Pan J-W 2012 *Phys. Rev. Lett.* **109** 115301
 - [8] Dalibard J, Gerbier F, Juzeliūnas G and Öhberg P 2011 *Rev. Mod. Phys.* **83** 1523
 - [9] Zhai H 2015 *Rep. Prog. Phys.* **78** 026001
 - [10] Ho T-L and Zhang S 2011 *Phys. Rev. Lett.* **107** 150403
 - [11] Sinha S, Nath R and Santos L 2011 *Phys. Rev. Lett.* **107** 270401
 - [12] Hu H, Ramachandran B, Pu H and Liu X-J 2012 *Phys. Rev. Lett.* **108** 010402
 - [13] Li Y, Pitaevskii L P and Stringari S 2012 *Phys. Rev. Lett.* **108** 225301
 - [14] Kawakami T, Mizushima T, Nitta M and Machida K 2012 *Phys. Rev. Lett.* **109** 015301
 - [15] Zhang Y, Mao L and Zhang C 2012 *Phys. Rev. Lett.* **108** 035302
 - [16] Ruokokoski E, Huhtamäki J A M, and Möttönen M 2012 *Phys. Rev. A* **86** 051607(R)
 - [17] Zhu Q, Zhang C and Wu B 2012 *EPL* **100** 50003
 - [18] Huang L, Meng Z, Wang P, Peng P, Zhang S-L, Chen L, Li D, Zhou Q and Zhang J 2016 *Nature Phys.* **12** 540
 - [19] Wu Z, Zhang L, Sun W, Xu X-T, Wang B-Z, Ji S-C, Deng Y, Chen S, Liu X-J and Pan J-W 2016 *Science* **354** 83
 - [20] Xu X-Q and Han J H 2011 *Phys. Rev. Lett.* **107** 200401
 - [21] Radić J, Sedrakyan T A, Spielman I B and Galitski V 2011 *Phys. Rev. A* **84** 063604
 - [22] Zhou X-F, Zhou J and Wu C 2011 *Phys. Rev. A* **84** 063624
 - [23] Ramachandran B, Opanchuk B, Liu X-J, Pu H, Drummond P D and Hu H 2012 *Phys. Rev. A* **85** 023606
 - [24] Liu C-F, Fan H, Zhang Y-C, Wang D-S and Liu W-M 2012 *Phys. Rev. A* **86** 053616
 - [25] Aftalion A and Mason P 2013 *Phys. Rev. A* **88** 023610
 - [26] Xu Z-F, Kobayashi S and Ueda M 2013 *Phys. Rev. A* **88** 013621
 - [27] Fetter A L 2014 *Phys. Rev. A* **89** 023629
 - [28] Ueda M 2010 *Fundamentals and New Frontiers of Bose-Einstein Condensation* (Singapore: World Scientific)
 - [29] Wu B and Niu Q 2001 *Phys. Rev. A* **64** 061603(R)
 - [30] Wen L, Xiong H and Wu B 2010 *Phys. Rev. A* **82** 053627
 - [31] Kasamatsu K, Tsubota M and Ueda M 2002 *Phys. Rev. A* **66** 053606
 - [32] Wen L, Zhu Q, Xu T, Jing X and Liu C 2016 *J. Phys. B* **49** 015303
 - [33] Ryu C, Andersen M F, Cladé P, Natarajan V, Helmerson K and Phillips W D 2007 *Phys. Rev. Lett.* **99** 260401
 - [34] Beattie S, Moulder S, Fletcher R J and Hadzibabic Z 2013 *Phys. Rev. Lett.* **110** 025301
 - [35] Corman L, Chomaz L, Bienaimé T, Desbuquois R, Weitenberg C, Nascimbène S, Dalibard J and Beugnon J 2014 *Phys. Rev. Lett.* **113** 135302
 - [36] Eckel S, Lee J G, Jendrzejewski F, Murray N, Clark C W, Lobb C J, Phillips W D, Edwards M and Campbell G K 2014 *Nature (London)* **506** 200
 - [37] Wood A A, McKellar B H J and Martin A M 2016 *Phys. Rev. Lett.* **116** 250403
 - [38] Cozzini M, Jackson B and Stringari S 2006 *Phys. Rev. A* **73** 013603
 - [39] Mizushima T, Machida K and Kita T 2002 *Phys. Rev. Lett.* **89** 030401.
 - [40] Kasamatsu K, Tsubota M and Ueda M 2004 *Phys. Rev. Lett.* **93** 250406
 - [41] Peaceman D W and Rachford H H 1955 *J. Soc. Ind. Appl. Math.* **3** 28
 - [42] Wen L, Qiao Y, Xu Y and Mao L 2013 *Phys. Rev. A* **87** 033604
 - [43] Mithun T, Porsezian K and Dey B 2014 *Phys. Rev. A* **89** 053625
 - [44] Wen L and Li J 2014 *Phys. Rev. A* **90** 053621
 - [45] Zhou X-F, Zhou Z-W, Wu C and Guo G-C 2015 *Phys. Rev. A* **91** 033603
 - [46] Matthews M R, Anderson B P, Haljan P C, Hall D S, Wieman C E and Cornell E A 1999 *Phys. Rev. Lett.* **83** 2498
 - [47] Anderson P W and Toulouse G 1977 *Phys. Rev. Lett.* **38** 508
 - [48] Skyrme T H R 1962 *Nucl. Phys.* **31** 556
 - [49] Zhai H, Chen W Q, Xu Z and Chang L 2003 *Phys. Rev. A* **68** 043602
 - [50] Kasamatsu K, Tsubota M and Ueda M 2005 *Phys. Rev. A* **71** 043611

- [51] Yang S-J, Wu Q-S, Zhang S-N and Feng S 2008 *Phys. Rev. A* **77** 033621
- [52] Fetter A L 2009 *Rev. Mod. Phys.* **81** 647
- [53] Zhang X-F, Kato M, Han W, Zhang S-G and Saito H 2016 arXiv:1610.09458
- [54] White A C, Zhang Y and Busch T 2016 arXiv:1612.01713